CONF-790306--4

LA-UR -78-2933

TITLE: DESIGN AND PERFORMANCE OF SODIUM-BONDED URANIUM-PLUTONIUM CARBIDE FUEL ELEMENTS

AUTHOR(S): J. F. Kerrisk (LASL)
N. S. DeMuth (LASL)
R. L. Petty (LASL)
T. W. Latimer (LASL)
J. A. Vitti (AI)
L. J. Jones (AI)

MASTER

SUBMITTED TO:

Monterey International Conference on
Fast Breeder Reactor Fuel Performance
March 5-8, 1979

los alamos
scientific laboratory
of the University of California
LOS ALAMOS, NEW MEXICO 87545

An Affirmative Action/Equal Opportunity Employer

Form No. 836
St. No. 2629
1/75

UNITED STATES
ENERGY RESEARCH AND
DEVELOPMENT ADMINISTRATION
CONTRACT W-7405-ENG-36

DESIGN AND PERFORMANCE OF SODIUM-BONDED URANIUM-PLUTONIUM CARBIDE FUEL ELEMENTS

J. F. Kerrisk, N. S. DeMuth, R. L. Petty, T. W. Latimer (LASL)
J. A. Vitti and L. J. Jones (AI)

INTRODUCTION

The introduction of advanced carbide fuels into commercial liquid-metal fast breeder reactors (LMFBR) has the potential for providing a system with high breeding ratio and low fuel-cycle costs. Sodium-bonded elements with (U,Pu)C fuel comprise one of the major designs currently being pursued in the advanced fuels program. The general objective of the program is to establish the irradiation performance of elements with design parameters and operating conditions that are characteristic of LMFBRs with high breeding ratios. This paper summarizes the design and irradiation performance of sodium-bonded elements with carbide fuel and describes one type of high-performance core that can be designed with these elements.

The general philosophy used in designing sodium-bonded elements is to size the fuel-cladding gap to accommodate fuel swelling during the lifetime of the element. High-density fuel, generally greater than 98% of theoretical density, is employed so as to concentrate space for swelling in the gap. The sodium bond provides a good heat-transfer medium that keeps fuel temperatures low compared to helium-bonded elements. These design features give sodium-bonded elements a potential for achieving high burnup at high linear power. However, early irradiation tests indicated that fuel-pellet cracking, followed by rearrangement and wedging of the broken fuel pieces, led to fuel-cladding mechanical interaction early in life.[1] This may have been the primary cause of cladding failure in these early tests. Numerous solutions to the problem were considered. Fuel-fragment restraint devices (shroud tubes) were given primary attention.[2] The use of cladding that was thicker and stronger than that employed in early tests was also tried. Specific tests that compare the irradiation performance of elements with and without shroud tubes, with different fuel and cladding compositions, and under a variety of operating conditions are being performed.

CURRENT TEST PROGRAM

A summary of the sodium-bonded carbide tests in the current program is given in Table I. All are EBR-II tests. The first three (U5100, K4, and K4B) had a large number of variables and were, to some extent, scoping tests. The primary objectives of these tests were to compare the irradiation performance of elements with varying amounts of sesquicarbide in the fuel (U5100, K4, and K4B), with and without shroud tubes (U5100), with different designs of shroud tubes (U5100 and K4), and with various cladding and shroud-tube materials (U5100). The fuel in these experiments varied from single-phase (U,Pu)C to fuel with as much as 17 vol% sesquicarbide. The U5100 elements without shroud tubes attained only ~3 at.% burnup when one failed. The remaining U5100 elements continued irradiation with the K4 test. The shroud tube designs in the U5100 and K4 elements varied mainly in the slot area in the tubes.[2] The U5100-element claddings were solution-annealed Type 304 stainless steel and Incoloy 800 with 0.36-mm wall thickness. Both the K4 and K4B tests used 20% cold-worked Type 316 stainless steel cladding, 0.30-mm thick for K4 and 0.38-mm thick for K4B.

In the latter six tests (AIR-1 and K7 through K12), all fuel was $(U_{0.8}Pu_{0.2})C$ with 10 ± 5 vol% $(U,Pu)_2C_3$. Most of the tests (AIR-1, K7, K8, and K9) were clad in 20% cold-worked Type 316 stainless steel; one (K11) had Nimonic PE16 and Type-316-stainless-steel claddings while another (K12) had only PE16 cladding. Two cladding diameters were employed (see Table I). Most tests (AIR-1 and K7 through K11) used 0.38-mm-thick cladding for elements with shroud tubes and 0.51-mm-thick cladding for elements without shroud tubes. In K12, the cladding was reduced to a wall thickness of 0.30 mm for elements with shroud tubes and 0.38 mm for elements without shroud tubes because of the increased strength of PE16 over that of stainless steel. Two of these tests (AIR-1 and K12) were designed to compare the behavior of elements with and without shroud tubes. These tests used both 20% cold-worked and solution-annealed Type-316-stainless-steel shroud-tube material. All sodium-bonded elements in the other four tests had shroud tubes; two (K7 and K8) employed only cold-worked material while the other two (K9 and K11) used both cold-worked and solution-annealed material. Wall thicknesses of the shroud tubes were 0.08-0.09 mm. Diametral gap sizes are listed in Table I.

The operating conditions of these experiments were designed to simulate two LMFBR core locations: near the core midplane where peak power occurs, and at the top of the core where the power is low but the cladding temperature is high. The short core height (343 mm) and relatively flat axial power profile of EBR-II did not permit achieving typical LMFBR peak-power and top-of-core conditions in a single test. Two tests (K8 and K9) simulate top-of-core conditions with peak cladding temperatures near 650°C (see Table I). The peak linear powers of these two tests depend on the

TABLE I

Sodium Bonded Carbide Tests

Test	Experiment Fabricator	Number of Elements Total	Number of Elements With Shrouds	Element Diameter (mm)	Diametral[a] Gap (mm)	Peak Cladding Temp. (°C)	Peak Linear Power (kW/m)	Peak[b] Burnup (at.%)	Goal Burnup (at.%)	Current[b] Status
U5100	GUNFC	18	7	7.87	0.65 (S) 0.4/0.8 (U)	615	72-74[c]	3.0-8.9	9	Examination
K4	LASL	8	8	7.87	0.62	615	80-90	5.6-9.5	9	Examination
K4B	LASL	4	4	7.87	0.65	615	72-75	3.7-3.8	9	Irradiation
AIR-1	AI/LASL	23	10	7.87	0.64 (S) 0.56 (U)	565	76-86	8.0-11.3	12	Examination
K7	LASL	9	9	7.87	0.64	595	62-72	3.1-8.5	12	Irradia.
K8	LASL	6	6	7.87	0.64	650	45-46	3.8-4.0	8	Irradiation
K9	LASL	7	7	9.40	0.79	655	70-73	3.3-3.5	8	Irradiation
K11	LASL	19	19	9.40	0.79	595	93-105	5.2-5.7	12	Irradiation
K12	LASL	19	8	9.40	0.78 (S) 0.76/0.53 (U)	595	96-109	4.0-4.6	12	Irradiation

[a] S = Elements with shroud tubes and U = elements without.

[b] Completion of EBR-II Run 95 (August 1, 1978).

[c] Irradiated at 79-108 kW/m for initial 3 at.%.

element diameter; they were chosen to give top-of-core linear powers similar to those expected in the Fast Test Reactor (FTR). The other seven tests simulate the peak power conditions in FTR.

IRRADIATION PERFORMANCE

Three of the tests described in Table I (U5100, K4, and AIR-1) have reached their goal burnup and are in various stages of postirradiation examination. The remainder of the tests are continuing irradiation, although interim examinations have been performed on K4B, K7, K8, and K9 elements. One cladding failure has occurred in a K4 element that exceeded its goal burnup. Most of the irradiation-performance information is based on data from U5100 and K4 elements; however information from other elements obtained during interim examinations is also included.

Fuel Swelling

Fuel swelling rates have been estimated in two ways: from fuel column length changes and from measurements on whole, single fuel pellets taken near the midplane of the fuel columns of U5100 and K4 elements. Both types of measurements indicate that the unrestrained-swelling rate of single-phase monocarbide fuel is greater than that of fuel with sesquicarbide present. Peak fuel-swelling rates of ~3.0 vol%/at.% burnup were determined for single-phase (U,Pu)C while rates of ~2.4 vol%/at.% burnup were found for fuel with sesquicarbide present.

Shroud Tube Performance

Evidence from U5100 and K4 elements at interim and final examinations (5.6-9.5 at.% burnup) and AIR-1 elements at interim examination (~8 at.% burnup) indicates that shroud tubes are meeting their design requirement of retaining broken fuel fragments.[2] During the examination of the U5100 and AIR-1 elements and one low-burnup K4 element, the shroud tubes and associated fuel pellets were ejected from the cladding. Little or no force was required, indicating no mechanical interaction with the cladding. Some cracking of shroud-tube ligaments was seen, sometimes completely around the tube. Little evidence of chemical interaction between the fuel and shroud tubes was evident except for carburization and pitted areas in some stainless steel shroud-tube ligaments.[2]

During the final examination of the high-burnup K4 elements (8.8-9.5 at.%), attempts to eject the shroud tubes and fuel from the claddings of two elements were unsuccessful owing to the large forces encountered.

Profilometry data also gave indications of fuel-cladding mechanical interaction in these elements. When transverse metallographic sections were taken, the shroud tubes and fuel were nearly in contact with the cladding (Fig. 1). These elements appear to be examples of complete use of the available room for swelling with subsequent fuel-cladding mechanical interaction. The failed element (K4-2) was in this group; however, fuel-cladding mechanical interaction was probably not the sole cause of failure (see Cladding Deformation section).

Three tests (U510C, AIR-1, and K12) were designed to compare the irradiation behavior of elements with and without shroud tubes. The early failure (3 at.%) of a U510C element without a shroud tube was not unexpected since the design of these elements was not substantially different from early sodium-bonded elements that failed. The excellent performance of the U510C elements with shroud tubes indicates the value of the shroud tube in this design. The lack of failures in the AIR-1 test shows that when thicker (0.51-mm wall) and higher strength (20% cold-worked Type 316 stainless steel) cladding is used in sodium-bonded elements without shroud tubes, they can also achieve a high goal burnup.

Cladding Deformation

Cladding deformations associated with internal mechanisms (fuel-cladding mechanical interaction) and external mechanisms (spacer-cladding mechanical interaction) have been observed in sodium-bonded elements. Cladding ovalities resulting from fuel cracking and rearrangement were a common occurrence in early sodium-bonded elements without shroud tubes.[3] These ovalities were irregularly spaced axially along the cladding. Ovalities caused by fuel-cladding mechanical interaction are usually absent in elements with shroud tubes. The high-burnup K4 elements, however, showed that fuel-cladding mechanical interaction can occur late in life, when the gap available for swelling is used up. In addition to ovalities, this mechanical interaction has caused periodic variations in the average cladding diameter that relate to fuel-pellet locations (Fig. 2).

Most of the early irradiation test elements were individually encapsulated, which eliminated external forces on the element cladding. The U510C, K4, K4B, and K7 tests had the first elements with wire-wrapped spacers. The effects of spacer wire-cladding mechanical interaction were seen as spiral ovalities in the cladding of these elements.[4] The ovalities were probably caused by tightening of the wire wrap on individual elements as a result of differential thermal expansion and swelling. The cladding ovalities were very large (up to 0.2 mm) in some U510C elements at ~9 at.% burnup, smaller (less than 0.1 mm) in the K4 elements of comparable burnup, and much smaller in the K4B and K7 elements that were only at ~4 at.% burnup. The axial variation of the ovality size, as well as the variation with

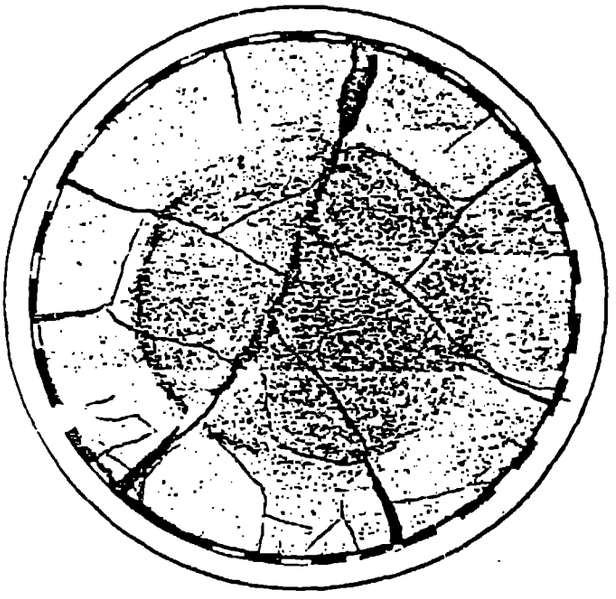

Fig. 1. Transverse section from element K4-2 near the failure location.

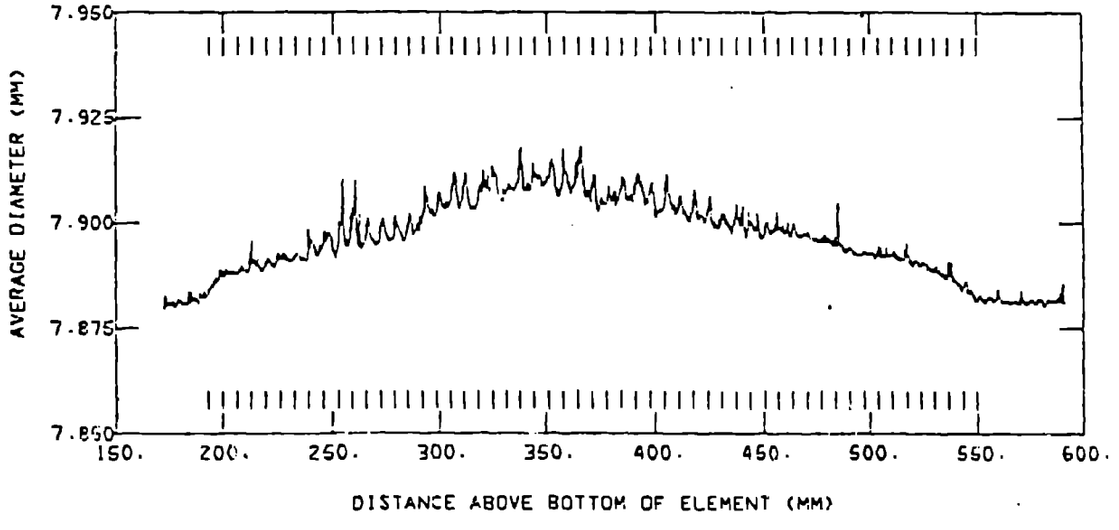

Fig. 2. Average cladding diameter of element K4-1. Vertical ticks at the top and bottom of the plot represent axial locations of pellet interfaces.

cladding material, indicated that irradiation-enhanced creep is the predominant inelastic-deformation mechanism. The AIR-1 elements were not wire wrapped but were contained in individual flow shroud tubes with indentations to center the elements (A19-B subassembly). Four elements removed for interim examination at ~8 at.% burnup had some periodic cladding ovalities that may be related to the spacer system as well as some irregularly spaced ovalities. All ovalities were small (less than 0.05 mm) except for one element that had become oval over the entire fuel column.

The cladding crack in the failed K4 element (K4-2) was located under the wire wrap where the wire contacted the subassembly wall. The wire had caused a local indentation in the outside surface of the cladding coincident with the crack (Fig. 3). Thus, in addition to fuel-cladding mechanical interaction, this element experienced significant spacer wire-cladding mechanical interaction in the vicinity of the cladding crack.

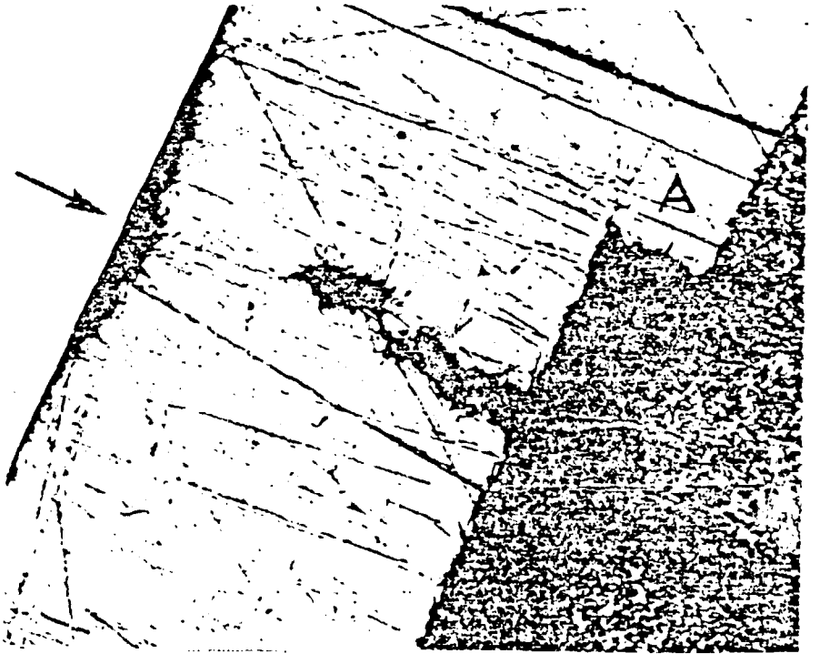

Fig. 3. Partial transverse section from element K4-2 showing the cladding crack and indentation (arrow) from the wire wrap. The shroud tube is located at A. As ground.

Cladding Carburization

Cladding carburization has been determined from hardness measurements made on transverse sections of cladding from a number of elements (U5100 and K4). The inner cladding surface was hardened up to 0.11 mm in depth when sesquicarbide was present in the fuel. Single-phase (U,Pu)C fuel appeared to cause very little cladding carburization (Fig. 4, U253). Hardness profiles and depths were similar for Type 316 stainless steel (Fig. 4, K4-4) and Incoloy 800 (Fig. 4, U257 and U259). Depths were, in general, insensitive to the type of shroud material and to cladding temperatures in the range 400-600°C.

Fission-Gas Release

Fission gas released from the fuel during irradiation was measured during destructive examinations of U5100, K4, and AIR-1 elements. Releases ranged from 3 to 14% of the gas generated.

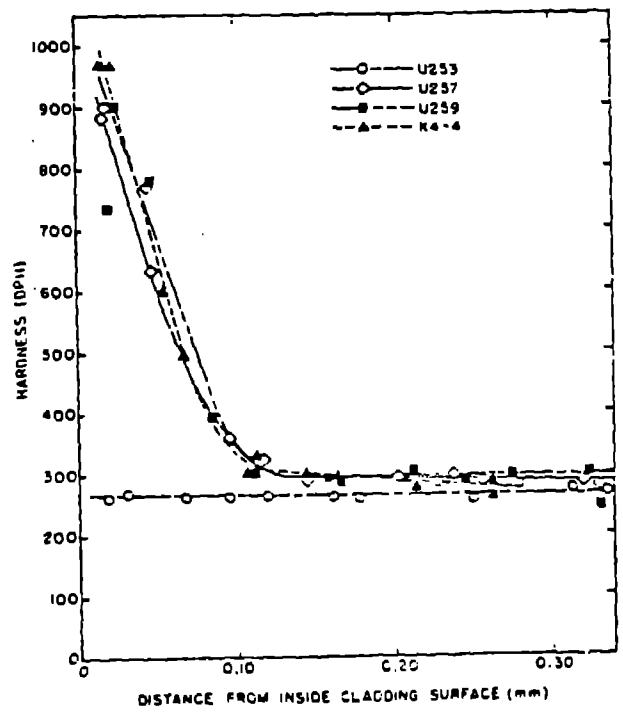

Fig. 4. Cladding hardness as a function of radial location near the midplane of elements U253, U257, U259, and K4-4.

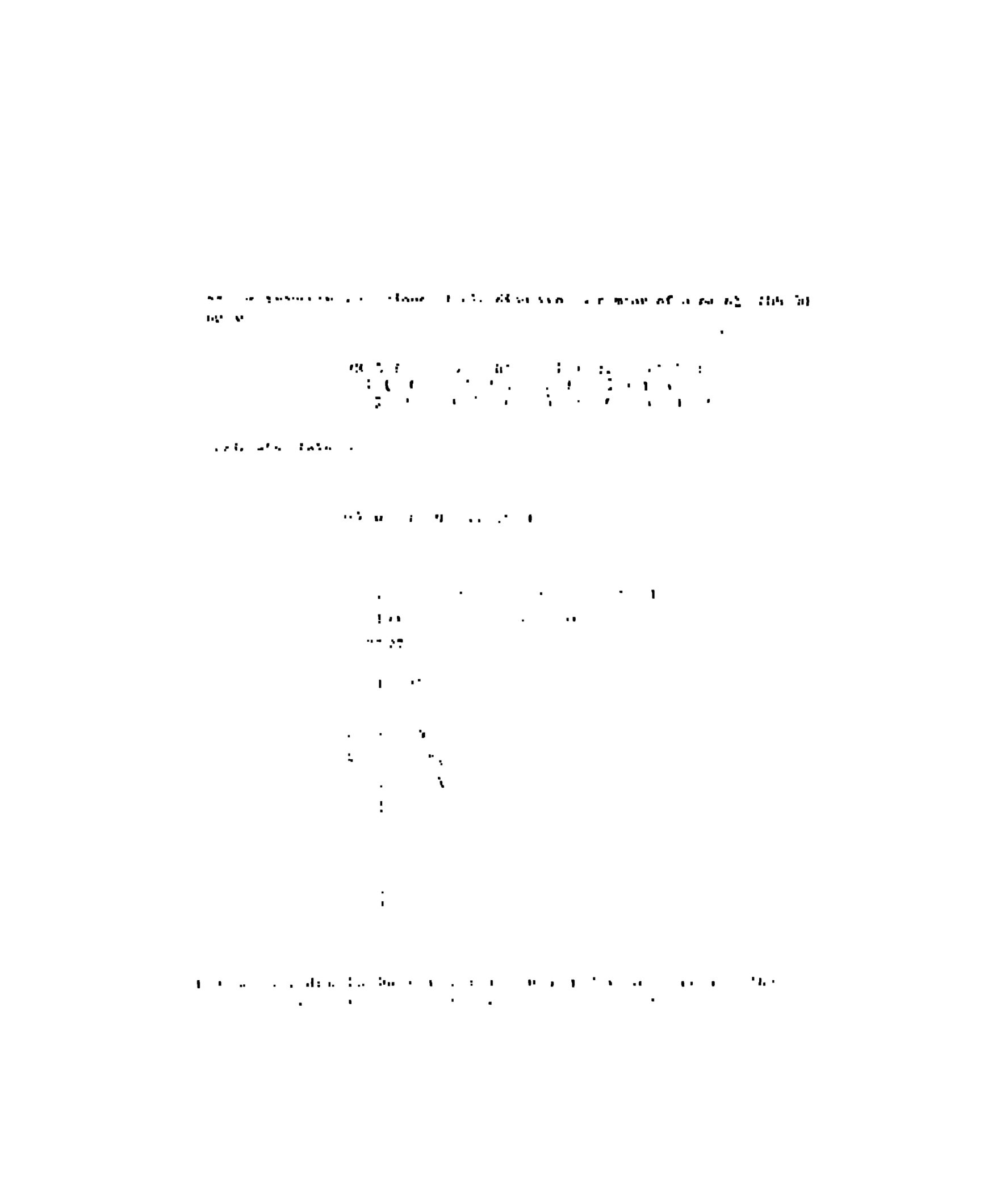

Overall Irradiation Performance

The irradiation performance of recent sodium-bonded fuel elements has been quite impressive. The failed element (K4-2) was beyond its goal burn-up at failure. Shroud tubes appear to be an effective means of reducing fuel-cladding mechanical interaction. Thicker and stronger cladding also appears to be a successful solution to this problem. Irradiation testing to date has demonstrated that sodium-bonded elements can perform reliably under LMFBR operating conditions.

CORE DESIGN

Utilizing the sodium-bonded carbide-fuel-element design demonstrated in the tests described above, a heterogeneous core has been designed for a 1000 MWe (2740 MWt) LMFBR.[5] The reactor has a fissile loading of 4670 kg at the beginning of the equilibrium cycle with a fissile gain of 353 kg/cycle. The fissile feed enrichment is 13.9% for Driver Rings 1 and 2 and is 15.5% for Driver Ring 3. The middle-of-equilibrium-cycle breeding ratio is 1.55, and the compound system stand-alone doubling time is less than 13 years. The end-of-equilibrium-cycle driver-region sodium-void reactivity worth was calculated to be \$2.74. The end-of-equilibrium-cycle Doppler coefficient ($-T\Delta K/\Delta T$) is 0.0049 for the driver fuel and is 0.0096 for drivers and all blankets. This core design, thus, provides outstanding performance combined with acceptable safety parameters, which should enhance its licensability.

The core is in a bull's-eye configuration, as depicted in Fig. 5, with 3 driver rings, a central blanket region, 2 annular blanket rings, and a radial blanket region, containing a total of 240 driver assemblies, 115 internal blanket assemblies, and 204 radial blanket assemblies. It uses 24 control/safety assemblies with enriched B_4C absorber rods. Two rings of steel reflector assemblies, 186 total, surround the radial blanket region to protect the reactor-system structure from irradiation damage. The active core height is 1.17 m with 0.79-m axial blankets.

Each driver assembly, as shown in Fig. 6, consists of a bundle of 169 wire-wrapped fuel elements (9.40-mm o.d. with 0.38-mm thick cladding) and a lower shield region inside a hexagonal duct, with an inlet nozzle at the bottom end and a handling socket at the top end. The driver elements are vertically supported at their lower ends on a series of supported bars. The elements in the outer ring of the bundles are wrapped with half-size wire wraps to decrease the edge-flow area. The proper power-to-flow ratio for assemblies in each flow-orifice zone is achieved by varying the number and size of orifice holes in the inlet nozzles. Raised spacer or load pads

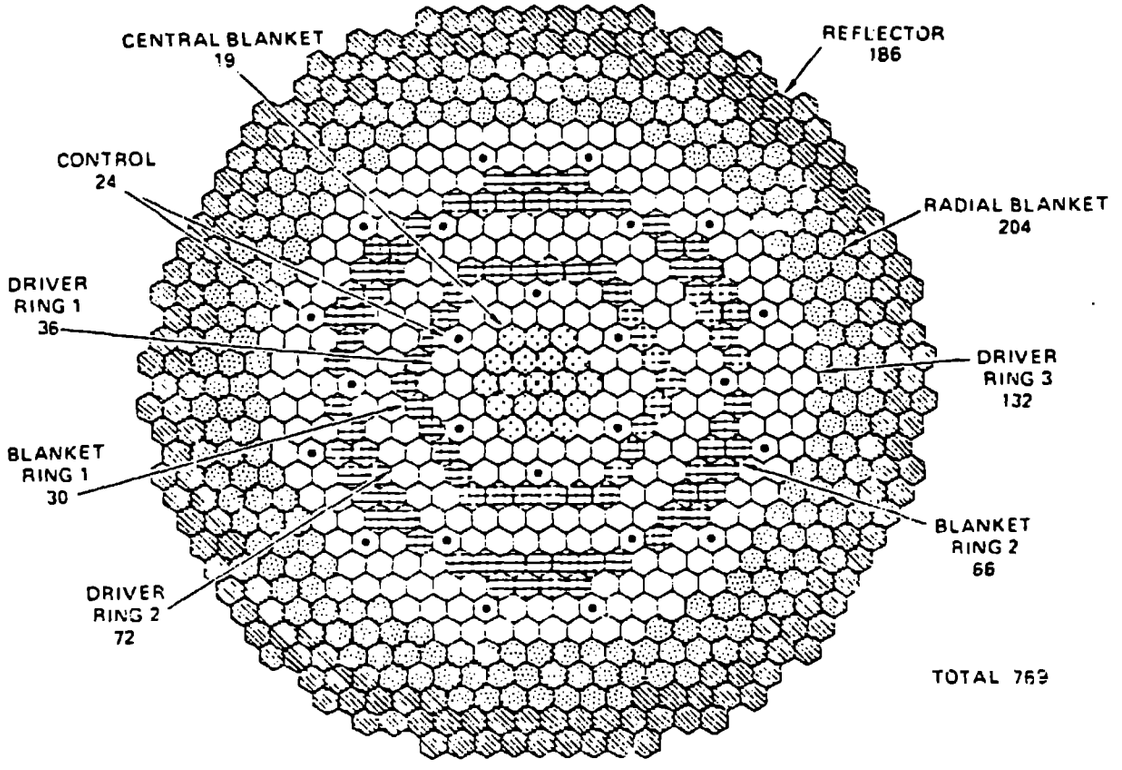

Fig. 5. Carbide-fueled bull's-eye core configuration.

on each assembly are located at two elevations above the active core. The pads establish a 6.9-mm gap between assemblies to accommodate bowing and dilation associated with irradiation swelling and creep of the duct walls.

The driver pins contain a 1.168-m stack of (U,Pu)C fuel pellets between 0.432 m of lower-blanket and 0.356 m of upper-blanket pellets. The fuel pins are sodium bonded and contain 0.813-m gas plenums immediately above the upper blanket for the collection of fission gases. The assembly duct and the element cladding material is an improved 20% cold-worked Type 316 stainless steel, which was used for the recently concluded DOE proliferation-resistant LMFBR design studies.[5]

The core contains two types of blanket assemblies, internal and radial. Both types contain 91 wire-wrapped blanket elements inside a 20% cold-worked, improved Type-316-stainless-steel duct. The blanket assemblies, as shown in Fig. 6, are slightly larger than the driver assemblies, and

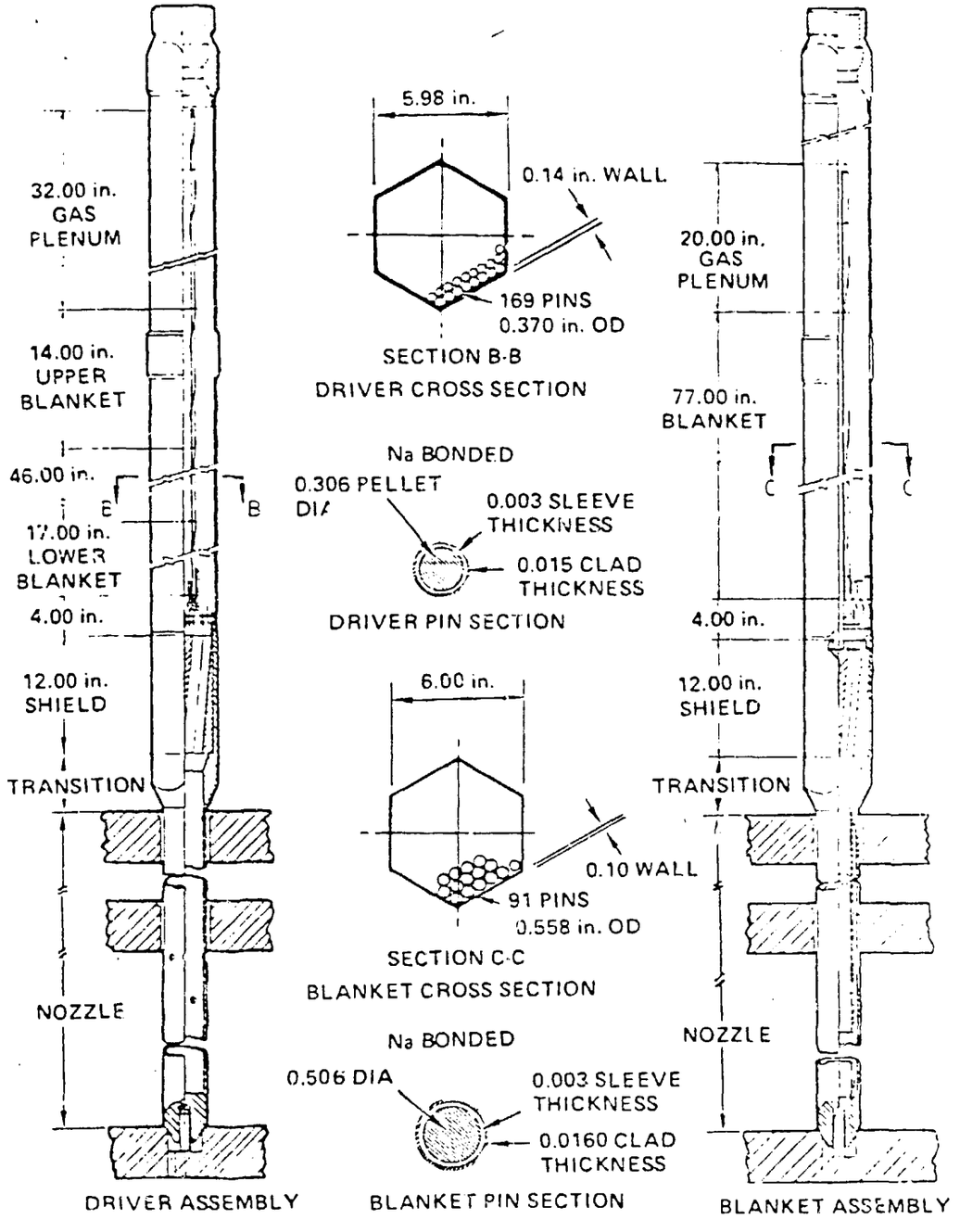

Fig. 6. Carbide driver and blanket assemblies.

the load pads establish a gap of only 6.4 mm between the blanket ducts. The radial-blanket elements contain a 1.651-m length of fertile material (UC), which is sodium bonded to improved 20% cold-worked, Type-316-stainless-steel cladding. The internal-blanket elements have 1.956-m-long fertile regions to match the driver-fuel plus axial-blanket lengths. Both blanket types have a 0.508-m upper fission-gas plenum. The peak linear power is 78 kW/m. The mixed-mean sodium-outlet temperature is 500°C with a 156°C reactor temperature rise. The peak discharge burnup of the fuel is 88 MWd/kg for a 3-year residence time.

SUMMARY

Recent results from irradiation tests indicate that sodium-bonded elements provide a practical advanced-fuel-element design for use in LMFBRs. Shroud tubes have effectively controlled fuel-cladding mechanical interaction; thicker and stronger claddings have also been effective in this respect. Burnups to 11 at.% have been achieved under typical operating conditions. A hetrogeneous core with a breeding ratio of 1.55 and a compound system doubling time of less than 13 years has been designed using these element designs.

REFERENCES

1. J. O. Barner, T. W. Latimer, J. F. Kerrisk, R. L. Petty, and J. L. Green, "Advanced Carbide Fuels-U.S. Experience," Advanced LMFBR Fuels, ERDA 4455, pp. 268-298 (1977).

2. J. F. Kerrisk, J. O. Barner, and R. L. Petty, "Design and Performance of Shroud Tubes in Sodium-Bonded Advanced Fuel Elements," Advanced LMFBR Fuels, ERDA 4455, pp. 648-659 (1977).

3. J. F. Kerrisk, J. O. Barner, and R. L. Petty, "Cladding Ovalities in Advanced Liquid-Metal Fast Breeder Reactor Fuel Elements," Nucl. Tech., 30, 361-375 (1976).

4. J. F. Kerrisk, R. L. Petty, N. S. DeMuth, and T. W. Latimer, "Wire Wrap-Cladding Mechanical Interaction in Sodium-Bonded Elements," Trans. Amer. Nucl. Soc., 30 (1978).

5. J. A. Vitti, L. D. Felten, J. C. Brittingham, N. G. Galluzzo, B. J. Ostermier, and A. V. von Arx, "Summary Report--Preconceptual Study of 1000 MWe Carbide-Fueled LMFBR Designs," ESG-DOE-13244 (September 1978).

A boson polynomial corresponding to a double standard Weyl tableau is defined as the product of the determinantal bosons (34) taken over all columns $1,2,\ldots,\lambda_1$ of the frame. Using the double Gel'fand pattern to denote the polynomials, we have:

$$P\begin{pmatrix}(m')\\[m]\\(m)\end{pmatrix}(A) \equiv \prod_{k=1}^{\lambda_1} \begin{vmatrix} j_{1k} & \cdots & j_{\lambda'_k k} \\ a_{i_{1k}} & \cdots & a_{i_{\lambda'_k k}} \end{vmatrix} . \tag{35}$$

We note two special cases of Eq. (35)

$$P\begin{pmatrix}(m')\\[m]\\(max)\end{pmatrix}(A) = \prod_{k=1}^{n} \begin{pmatrix} 1 & 2 & \cdots & k \\ 1 & 2 & \cdots & k \end{pmatrix}^{m_{kn}-m_{k+1n}} , \tag{36}$$

$$P\begin{pmatrix}(max)\\[m]\\(semi\text{-}max)\end{pmatrix}(A) = \prod_{k=1}^{n-1} \begin{pmatrix} 1 & 2 & \cdots & k \\ 1 & 2 & \cdots & k \end{pmatrix}^{m_{kn-1}-m_{k+1n}} \tag{37}$$

$$\times \prod_{k=1}^{n} \begin{pmatrix} 1 & 2 & \cdots & k-1 & k \\ 1 & 2 & \cdots & k-1 & n \end{pmatrix}^{m_{kn}-m_{kn-1}} ,$$

where $m_{ij} \equiv 0$ for $i > j$, $\begin{pmatrix} 1 & 2 & \cdots & k-1 & k \\ 1 & 2 & \cdots & k-1 & n \end{pmatrix} \equiv a^k_n$ for $k=1$, and special pattern notations have been introduced:

$$\begin{pmatrix}[m]\\(max)\end{pmatrix} \equiv \begin{pmatrix} m_{1n} & m_{2n} & \cdots & m_{n-1n} & m_{nn} \\ \ddots & \ddots & & & \\ & m_{1n} & & m_{2n} & \\ & & & m_{in} & \end{pmatrix} , \tag{38}$$

$$\begin{pmatrix}m\\(semi\text{-}max)\\(max)\end{pmatrix} \equiv \begin{pmatrix} m_{1n} & m_{2n} & \cdots & m_{n-1n} & m_{nn} \\ & m_{1n-1} & m_{2n-1} & \cdots & m_{n-1n-1} \\ & & & (max) & \end{pmatrix} . \tag{39}$$

The weight (W,W') or content of the double standard tableau (32) [and of the double Gel'fand pattern (33) is defined to be [cf. Eqs. (1) and (9)]

$$(W,W') = (w_1,\ldots,w_n, w'_1,\ldots,w'_n) , \tag{40}$$

where (W) and (W') are, respectively, the weights of the left and right standard tableaux (upper and lower Gel'fand patterns).

As noted earlier the boson state vectors corresponding to the polynomials (35) are not, in general, orthogonal [cf. Eq. (44)-(46) below],

and the main emphasis in physics has been on the construction of *orthonormal basis vectors* denoted in the double Gel'fand pattern notation by

$$\left|\begin{pmatrix}(m')\\[m]\\(m)\end{pmatrix}\right> \equiv [M([m])]^{-\frac{1}{2}}\, B\begin{pmatrix}(m')\\m\\(m)\end{pmatrix}(A)\,|\,0> \tag{41}$$

where

$$M([m]) = H^{[m]} = \prod_{i=1}^{n} p_{ij}!\Big/ \prod_{i<j} (p_{in}-p_{jn}) \tag{42}$$

in which

$$p_{in} \equiv m_{in} + n-i \quad , \quad \begin{array}{l}(p_{in} \text{ is called a}\\ \text{"partial hook").}\end{array} \tag{43}$$

The boson polynomials

$$B\begin{pmatrix}(m')\\[m]\\(m)\end{pmatrix}(A) \tag{44}$$

occurring in Eq. (41) and the double tableau polynomials

$$P\begin{pmatrix}(m')\\[m]\\(m)\end{pmatrix}(A) \tag{45}$$

span the same vector spaces. However, only for the patterns

$$\begin{pmatrix}(max)\\[m]\\(max)\end{pmatrix} , \begin{pmatrix}(max)\\[m]\\(semi\text{-}max)\end{pmatrix} , \begin{pmatrix}(semi\text{-}max)\\[m]\\(max)\end{pmatrix} \tag{46}$$

do the polynomials agree (up to a normalization factor).

We will now state the form of the boson polynomials (44) referring to Refs. 11, 13, 17, and 23 for a discussion of the properties which characterize these orthonormal forms and for the derivations of the results below.

We begin with the statement of the simplest polynomials which are those corresponding to a Young frame having 1 row with p boxes so that [m] = [p0...0] = [p$\dot{0}$]

$$B\begin{pmatrix}(m')\\[p\,\dot{0}]\\(m)\end{pmatrix}(A) = \left[\prod_{i=1}^{n} (w_i)!\,(w_i')!\right]^{1/2} \times \sum_{\boxed{a}} \prod_{i,j=1}^{n} (\alpha_i^j)^{\alpha_i^j}/(\alpha_i^j)! \tag{47}$$

where [W] and [W'] denote the *weights* of the lower and upper Gel'fand patterns, respectively, and $\boxed{a}$ denotes the following square matrix of nonnegative integers with constraints on the sums of the entries in

$$\boxed{\alpha} = \begin{array}{|ccc|c} \alpha_1^1 & \alpha_1^2 \cdots & \alpha_1^n & w_1 \\ \alpha_2^1 & \alpha_2^2 \cdots & \alpha_2^n & w_2 \\ \multicolumn{3}{c|}{\vdots} & \\ \alpha_n^1 & \alpha_n^2 \cdots & \alpha_n^n & w_n \\ \hline w_1' & w_2' & w_n' & \end{array} \qquad (48)$$

The symbols w_i (w'_j) written to the right of row i (below column j) designate that the entries in row i (column j) are constrained to add to w_i (w'_j). The sum over $\boxed{\alpha}$ in Eq. (47) is to be taken over all non-negative integers α_i^j (for i,j = 1,2,...,n) which satisfy these constraints.

The general result has a form similar to Eq. (47):

$$B\begin{pmatrix}(m')\\[m]\\(m)\end{pmatrix}(A) = M^{1/2}([m]) \sum_{\alpha} C\begin{pmatrix}(m')\\[m]\\(m)\end{pmatrix}(\alpha) \times \prod_{i,j=1}^{n} (\alpha_i^j)^{\alpha_i^j}/[(\alpha_k^j)!]^{1/2}; \qquad (49)$$

where the coefficients C in this result are given by

$$C\begin{pmatrix}(m')\\[m]\\(m)\end{pmatrix}(\alpha) = \left\langle \begin{pmatrix}[m]\\(m')\end{pmatrix} \middle| \left\langle [w \begin{matrix}(\Gamma_n)\\(\alpha_n)\end{matrix} \mathring{0}] \right\rangle \cdots \left\langle [w \begin{matrix}(\Gamma_2)\\(\alpha_2)\end{matrix} \mathring{0}] \right\rangle \left\langle [w \begin{matrix}(\Gamma_1)\\(\alpha_1)\end{matrix} \mathring{0}] \right\rangle \middle| (0) \right\rangle \qquad (50)$$

in which $\begin{pmatrix}[w_i & \mathring{0}]\\ & \alpha_i\end{pmatrix}$ denotes the Gel'fand pattern

$$\begin{pmatrix}[w_i & \mathring{0}]\\(\alpha_i)\end{pmatrix} = \begin{pmatrix} \alpha_i^1+\alpha_i^2+\ldots+\alpha_i^n & 0 \ldots 0 \\ \ddots & \vdots \\ & 0 \\ \alpha_i^1+\alpha_i^2 & \\ \ddots & \\ & \alpha_i^1 \end{pmatrix} \qquad (51)$$

where (Γ_k) is the operator pattern which is uniquely determined by the Δ pattern

$$[\Delta(\Gamma_k)] = [m_{1k}m_{2k}\ldots m_{kk}\mathring{0}] - [m_{1k-1}m_{2k-1}\ldots m_{k-1k-1}\mathring{0}] \; . \qquad (52)$$

We can not go into an explanation here of the general structure of the coefficients (50), but we will explain how they are calculated for the

special case of interest for S_n. It is sufficient here to note that the general coefficients (50) are explicitly known.

We complete this general discussion with several observations on the properties of the boson polynomial (49): *The important properties (i) and (ii) noted earlier (end of Sec. V) apply as stated to the double Gel'fand pattern polynomials*

$$B\begin{pmatrix}(m')\\[m]\\(m)\end{pmatrix}(A) \quad .$$

Property (iii) also generalizes to the group U(n), *where the rows and columns of the matrix* $B^{[m]}(A)$ *are now to be enumerated by the* U(n-1) *Gel'fand patterns* ((m),(m')). [Similar statements also apply to the polynomials (35).] *Finally, we have also the transformation property under the combined left and right translations of the boson matrix,*

$$A \to \tilde{U}\,A\,V, \quad U, V \in U(n) \quad , \tag{53}$$

given by

$$B\begin{pmatrix}(m')\\[m]\\(m)\end{pmatrix}(\tilde{U}AV) = \sum_{(\mu)(\mu')} D^{[m]}_{(\mu)(m)}(U)\,D^{[m]}_{(\mu')(m')}(V)\,B\begin{pmatrix}(\mu')\\[m]\\(m)\end{pmatrix}(A), \tag{54}$$

where ~ *denotes matrix transposition, and*

$$\{D^{[m]}(U) \mid U \in U(n)\} \tag{55}$$

is the (unitary) matrix representation of U(n) *obtained by the identification*

$$D^{[m]}_{(m)(m')}(U) = B\begin{pmatrix}(m')\\[m]\\(m)\end{pmatrix}(U) \quad . \tag{56}$$

VII. *The Young-Yamanouchi real, proper orthogonal irreducible representations of* S_n.

Let us begin by considering the Cayley n x n permutation representation of S_n. For this one lets P denote a permutation by the rule:

$$P = \begin{pmatrix}1 & 2 & \dots & n\\ i_1 & i_2 & \dots & i_n\end{pmatrix} \quad . \tag{57}$$

Then the correspondence

$$P \to [e_{i_1}\, e_{i_2} \dots e_{i_n}] \equiv I_P \quad , \tag{58}$$

where e_i denotes a unit column vector with 1 in row i and zeroes elsewhere - is a representation of S_n by nxn matrices.

Since the general boson polynomial admits of an interpretation of the argument A by an nxn indeterminate, it is a well-defined operation to replace A by I_p, in Eq. (49). One obtains

$$B\begin{pmatrix}(m')\\[m]\\(m)\end{pmatrix}(I_p)$$

$$= [M([m])]^{1/2}\delta_{w_1'w_{i_1}}\delta_{w_2'w_{i_2}}\cdots\delta_{w_n'w_{i_n}}\,C\begin{pmatrix}(m')\\[m]\\(m)\end{pmatrix}(a_p)\quad , \tag{59}$$

where a_p denotes the nxn numerical array

$$(a_p) = [w_{i_1}e_{i_1}, w_{i_2}e_{i_2},\ldots,w_{i_n}e_{i_n}] \quad . \tag{60}$$

Let us next specialize to representations having labels [m] which are partitions of n, and at the same time *restrict the two Gel'fand patterns* (m) *and* (m') *such that the weights* [W]=[W']=[i]. It follows at once from Eq. (59) that these special boson polynomials take the form:

$$B\begin{pmatrix}(m')\\[m]\\(m)\end{pmatrix}(I_p) = [M([m])]^{1/2}\,C\begin{pmatrix}(m')\\[m]\\(m)\end{pmatrix}(I_p) \quad . \tag{61}$$

It is useful to give a special notation to these objects; let us define

$$D^{[m]}_{(m),(m')}(P) = B\begin{pmatrix}(m')\\[m]\\(m)\end{pmatrix}(I_p) \quad . \tag{62}$$

Then

$$\{D^{[m]}(P)\,|\,P\in S_n\} \tag{63}$$

is an irreducible real, orthogonal representation of S_n.

Consider now the specific form taken by the matrix elements of these irreps. From Eq. (50) we obtain

$$D^{[m]}_{(m),(m')}(P) = [n!/\dim[m]]^{1/2}\times\left\langle\left(\begin{matrix}[m]\\(m)\end{matrix}\right)\middle|\left\langle\begin{matrix}[1 & \dot{0}]\\ i_n\end{matrix}\right\rangle\cdots\left\langle\begin{matrix}[1 & \dot{0}]\\ i_2\end{matrix}\right\rangle\left\langle\begin{matrix}[1 & 0]\\ i_1\end{matrix}\right\rangle\middle|\left|\begin{matrix}[\dot{0}]\\(0)\end{matrix}\right\rangle\right.$$

$$\text{for } P = \begin{pmatrix}1 & 2 & \cdots & n\\ i_1 & i_2 & \cdots & i_n\end{pmatrix}\quad , \tag{64}$$

where dim[m] denotes the dimension of the irreducible representation [m] of S_n. We shall now explain in detail the meaning of the quanti-

(i) The symbol

$$\left\langle \begin{matrix} & & \gamma & \\ [1 & & & \dot{0}] \\ & i & & \end{matrix} \right\rangle \tag{65}$$

denotes a *fundamental Wigner operator* of U(n) [cf. Refs. 9, 17, 18] in which $\begin{pmatrix} 1 & \dot{0} \\ i & \end{pmatrix}$ is an abbreviated notation for the n-rowed Gel'fand pattern which has weight [0 ...0 1 0...0] with the 1 appearing in position i; similarly, $\begin{pmatrix} & \gamma & \\ 1 & & 0 \end{pmatrix}$ denotes the inverted Gel'fand pattern which has weight [0...0 1 0...0] with the 1 appearing in position γ. Thus, we have:

$$i,\gamma = 1,2,\ldots,n \tag{66}$$

in the symbol (65). For example, for n=2, there are 9 fundamental Wigner operators, a typical example being

$$\left\langle \begin{matrix} & & \dot{0} \\ 1 & 2 & \\ & 1 & \end{matrix} \right\rangle = \left\langle \begin{matrix} & 1 & & 0 & \\ 1 & & 0 & & 0 \\ & 1 & & 0 & \end{matrix} \right\rangle \quad . \tag{67}$$

[We will see below that, while upper and lower patterns in Eq. (65) run over the same numerical patterns, the role of the two patterns in the definition of a fundamental Wigner operator (65) are qualitatively different.]

(ii) The sequence in integers

$$(\gamma_n, \gamma_{n-1}, \ldots, \gamma_1) \tag{68}$$

appearing in the upper patterns in Eq. (64) is the Yamanouchi symbol of the Gel'fand pattern

$$\begin{pmatrix} [m] \\ (m') \end{pmatrix} \quad . \tag{69}$$

[Cf. Eqs. (12) and (13).]

Our remaining task is to define the concept of a fundamental Wigner operator in U(n) and to show how the coefficients in Eq. (64) are calculated.

Let $H^{[m]}$ denote a carrier space for irreducible representation [m] of U(n). Then an orthonormal basis of the space $H^{[m]}$ is:

$$\left\{ |(m)\rangle \quad \begin{matrix} \text{(m) is a Gel'fand pattern of the} \\ \text{Young frame } Y_{[m]} \end{matrix} \right\} \quad . \tag{70}$$

The fundamental Wigner operator denoted by

$$\left\langle \begin{matrix} & & \tau & \\ [1 & & & \dot{0}] \\ & i & & \end{matrix} \right\rangle \tag{71}$$

is a mapping $H^{[m]} \to H^{[m]+\Delta(\tau)}$, where $\Delta(\tau)$ is the weight of the pattern

$(^{1}_{\tau}\dot{0})$. [If $m_{\tau n}+1 < m_{\tau+1,n}$, then $H^{[1n]+\Delta(\tau)}$ contains only the zero vector.] The mapping (71) is now defined explicitly by giving its action on each basis vector (70) of $H^{[m]}$:

$$\left\langle [1^{\tau}_{i}\dot{0}] \right\rangle \left| \begin{matrix}[m]\\(m)\end{matrix} \right\rangle = \sum_{(m')} \left\langle \begin{matrix}[m]+\Delta(\tau)\\(m')\end{matrix} \right| \left\langle [1^{\tau}_{i}\dot{0}] \right\rangle \left| \begin{matrix}[m]\\(m)\end{matrix} \right\rangle \times \left| \begin{matrix}[m]+\Delta(\tau)\\(m')\end{matrix} \right\rangle , \qquad (72)$$

where

$$\left\langle \begin{matrix}[m]+\Delta(\tau)\\(m')\end{matrix} \right| \left\langle [1^{\tau}_{i}\dot{0}] \right\rangle \left| \begin{matrix}[m]\\(m)\end{matrix} \right\rangle \qquad (73)$$

denotes a real number (matrix element) which we now describe.

For the description of the numbers (73), we require a detailed notation for the entries in the rows of a Gel'fand pattern. We introduce the notation $[m]_k = [m_{1k}\ldots m_{kk}]$ for the entries in row k, the notation $[1\ \dot{0}]_k$ for the row vector $[1\ 0\ldots0]$ of length k, and $\Delta_k(\tau_k)$ for the row vector of length k which has 1 in position τ_k $(1 \leq \tau_k \leq k)$ and zeroes elsewhere. In terms of this notation each matrix element (73) may be described in the following manner: Each matrix element (73) is zero unless the Gel'fand pattern

$$\begin{pmatrix}[m]+\Delta(\tau)\\(m')\end{pmatrix}$$

has the form

$$\begin{pmatrix} [m]_n + \Delta_n(\tau_n) \\ [m]_{n-1} + \Delta_{n-1}(\tau_{n-1}) \\ \vdots \\ [m]_i + \Delta_i(\tau_i) \\ [m]_{i-1} \\ \vdots \\ [m]_1 \end{pmatrix} , \qquad (74)$$

where for each prescribed pair, τ and i $(1 \leq \tau \leq n,\ 1 \leq i \leq n)$, the sequence of integers $\tau_n, \tau_{n-1}, \ldots, \tau_i$ satisfies

$$\tau_n = \tau \text{ and } 1 \leq \tau_k \leq k \text{ for } k = n-1,\ldots,i. \qquad (75)$$

Denoting the Gel'fand pattern (74) by the notation

$$\begin{pmatrix}[m]\\(m)\end{pmatrix}_{\tau_n\ldots\tau_i} , \qquad (76)$$

we have the result that each of the nonzero matrix elements (73) factor-

izes in the following manner:

$$\left\langle \begin{pmatrix} [m] \\ (m) \end{pmatrix}_{\tau_n \cdots \tau_i} \middle| \left\langle \begin{matrix} \tau \\ [1 \quad \dot{0}] \\ i \end{matrix} \right\rangle \middle| \begin{matrix} [m] \\ (m) \end{matrix} \right\rangle \tag{77}$$

$$= \prod_{k=i}^{n} \left\langle \begin{matrix} [m]_k + \Delta_k(\tau_k) \\ [m]_{k-1} + \Delta_{k-1}(\tau_{k-1}) \end{matrix} \middle| \begin{bmatrix} \tau_k \\ [1 \quad \dot{0}]_k \\ \tau_{k-1} \end{bmatrix} \middle| \begin{matrix} [m]_k \\ [m]_{k-1} \end{matrix} \right\rangle ,$$

in which, by convention, $\tau_{i-1} = i$ and $\Delta_{i-1}(i) = [\dot{0}]_{i-1}$.

Each of the real numbers

$$\left\langle \begin{matrix} [m]_k + \Delta_k(\tau_k) \\ [m]_{k-1} + \Delta_{k-1}(\tau_{k-1}) \end{matrix} \middle| \begin{bmatrix} \tau_k \\ [1 \quad \dot{0}]_k \\ \tau_{k-1} \end{bmatrix} \middle| \begin{matrix} [m]_k \\ [m]_{k-1} \end{matrix} \right\rangle \tag{78}$$

in the product (77) is called a *reduced* U(k): U(k-1) *matrix element* and has a very simple interpretation in terms of the *pattern calculus rules* developed in Ref. 7. We state these rules here for the special case required to evaluate the factor (78):

The pattern calculus rules (cf. Ref. 14).

(i) Write out two rows of dots and assign the numerical entries of $\Delta_k(\tau_k)$ and $\Delta_{k-1}(\tau_{k-1})$, as shown:

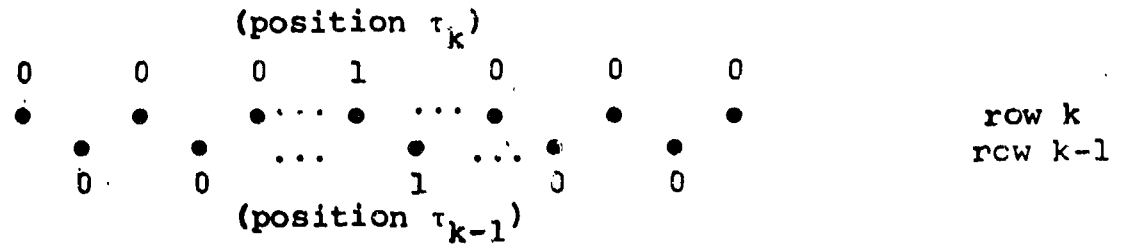

(ii) Draw an arrow between each point labelled by 1 (tail of arrow) to each point labelled by 0 (head of arrow). Once this arrow-pattern is drawn, remove the 0's and 1's from the diagram.

(iii) In the arrow-pattern assign the partial hook p_{ik} to point i (i=1,2,...,k from left to right) of row k and the partial hook p_{ik-1} to point i (i=1,2,...,k-1) in row k-1 ($p_{ij} \equiv m_{ij} + j - i$).

(iv) Assign a numerical factor to each arrow in the arrow-pattern using the rule

$$p_{tail} - p_{head} + e_{tail} ,$$

where $e_{tail}=1$ if the tail of the arrow is on row k-1 and $e_{tail}=0$ if tail of the arrow is on row k.

(v) Write out the products

N = product of all factors for arrows going *between* rows,

D = product of all factors for arrows going *within* rows.

The reduced U(k):U(k-1) matrix element (78) is then given by

$$S(\tau_{k-1}-\tau_k)\left[\frac{N}{D}\right]^{1/2}, \tag{79}$$

where $S(\tau_{k-1}-\tau_k)$ is +1 for $\tau_{k-1} > \tau_k$ and -1 for $\tau_{k-1}<\tau_k$.

Example. For k=3, τ_3=1, τ_2=2 the arrow-pattern is

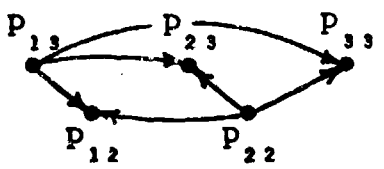

and the reduced matrix element (78) has the value given by

$$\left\langle \begin{matrix} m_{13}+1 & m_{23} & m_{33} \\ & m_{12} & m_{22}+1 \end{matrix} \middle| \begin{bmatrix} 1 & 1 & 0 & 0 & 0 \\ 1 & 1 & 0 & 0 & 0 \end{bmatrix} \middle| \begin{matrix} m_{13} & & m_{23} & & m_{33} \\ & m_{12} & & m_{22} & \end{matrix} \right\rangle$$

$$= -\left[\frac{(p_{13}-p_{12})(p_{22}-p_{33}+1)(p_{22}-p_{33}+1)}{(p_{13}-p_{23})(p_{13}-p_{33})(p_{22}-p_{12}+1)}\right]^{1/2}. \tag{80}$$

The result of applying these rules to Eqs. (78) is:

$$S(\tau_{k-1}-\tau_k)\left[\prod_{\substack{s=1\\ s\neq\tau_k}}^{k}\frac{(p_{\tau_{k-1}k-1}-p_{sk}+1)}{(p_{\tau_k k}-p_{sk})}\prod_{\substack{t=1\\ t\neq\tau_{k-1}}}^{k-1}\frac{(p_{\tau_k k}-p_{tk-1})}{(p_{\tau_{k-1}k-1}-p_{tk-1}+1)}\right]^{1/2}. \tag{81}$$

Remarks. Using the above results from the pattern calculus, Eq. (64) *is a completely explicit general result, giving for each* $P\in S_n$, *every element of the irreducible matrix representation* $D^{[m]}(P)$.

Thus we have achieved our stated goal of obtaining the real orthogonal S_n irreps in an explicit, non-recursive, way. The techniques we have used, in particular the pattern calculus, seem to be a natural extension of the ideas underlying the concept of a "hook" (due to Nakayama, and to Frame, et al.[26]) as applied in "hook product" of the Hall-Robinson formula[27].

REFERENCES

1. I.M. Gel'fand and M.L. Tseitlin, Matrix Elements for the unitary groups, Dokl Akad. Hauk SSSR (1950), 825-828.
2. M. Weyl, Gruppentheorie und Quantenmechanik", Hirzel, Leipzig: 1st ed., 1928; 2nd ed., 1931, translated as "The Theory of Groups and Quantum Mechanics", by M.P. Robertson, Methuen, London, 1931; reissued Dover, New York, 1949.
3. A Young, Quantitative Substitutional Analysis, PLMS (1), I, 33 (1901), 97-146; II, 34 (1902), 361-397, PLMS (2) III, 28 (1928), 255-292; IV, 31 (1930), 253-272; V. ibid., 273-288; VI, 34 (1932), 196-230; VII, 36 (1933), 304-368, VIII, 37 (1934), 441-495; IX, 54 (1952), 218-253.
4. H. Weyl, "The Structure and Representations of Continuous Groups", Lectures at the Inst. for Adv. Study, Princeton, N.J., 1934-35 (unpublished). (Notes by R. Brauer.)
5. T. Yamanouchi, On the calculation of atomic energy levels IV, Proc. Phys.-Math. Soc. Japan 18 (1936), 623-640; On the construction of unitary irreducible representations of the symmetric group, ibid. 19 (1937), 436-450.
6. P. Doubilet, G.-C. Rota. and J. Stein, On the foundations of combinatorial theory: IX. Combinatorial methods in invariant theory, Studies in Appl. Math., Vol. LIII, No. 3, 1974, 185-216.
7. V. Bargmann and M. Moshinsky, Group thoery of harmonic oscillators (I). The collective modes, Nucl. Phys. 18 (1960), 697-712.
8. M. Moshinsky, Bases forthe irreducible representations of the unitary groups and some applications, J. Math. Phys. 4 (1963), 1128-1139.
9. G.E. Baird and L.C. Biedenharn, On the representations of semisimple Lie groups. II, J. Math. Phys. 4 (1963), 1449-1466; III, The explicit conjugation operation for SU(n), Ibid, 5 (1964), 1723-1730; IV, A canonical classification for tensor operators in SU_3, Ibid, 5 (1965), 1730-1747.
10. J.G. Nagel and M. Moshinsky, Operators that raise or lower the irreducible vector spaces of U_{n-1} contained in an irreducible vector space of U_n, J. Math. Phys. 6 (1965), 682-694.
11. J.D. Louck, Group theory of harmonic oscillators in n-dimensional space, J. Math. Phys. 6 (1965), 1786-1804.
12. M. Moshinsky, Gel'fand states and the irreducible representations of the symmetric group, J. Math. Phys. 7 (1966), 691-698.
13. L.C. Biedenharn, A. Giovannini, and J.D. Louck, Canonical definition of Wigner operators in U_n, J. Math. Phys. 8 (1967), 691-700.
14. L.C. Biedenharn and J.D. Louck, A pattern calculus for tensor operators in the unitary groups, Commun. Math. Phys. 8 (1968) 80-131.
15. P. Kramer and M. Moshinsky, Group theory of harmonic oscillators and nuclear structure, in "Group Theory and its Applications", ed. by E.M. Loebl, Academic Press, New York, 1968, 339-468.
16. M. Ciftan, On the combinatorial structure of state vectors in U(n), II. The generalization of hypergeometric functions on U(n) states, J. Math. Phys. 10 (1969), 1635-1646.
17. J.D. Louck, Recent progress toward a theory of tensor operators in the unitary groups, Am. J. Phys. 38 (1970), 3-42.
18. J.D. Louck and L.C. Biedenharn, Canonical unit adjoint tensor operators in U(n), J. Math. Phys. 11 (1970), 2368-2414.

19. A.C.T. Wu, Structure of the combinatorial generalization of hypergeometric functions for SU(n) states, J. Math. Phys. 12 (1971), 437-440
20. W.J. Holman, On the general boson states of U_n*U_n and Sp_4*Sp_4, Nuovo Cimento 4A (1971), 904-931.
21. W.J. Holman and L.C. Biedenharn, "The Representations and Tensor Operators of the Unitary Groups U(n)", in "Group Theory and its Applications", Vol. II, ed. by E.M. Loebl, Academic Press, New York, 1971, 1-73.
22. T.H. Seligman, The Weyl basis of the unitary group U(k), J. Math. Phys. 13 (1972), 876-879.
23. J.D. Louck and L.C. Biedenharn, The structure of the canonical tensor operators in the unitary groups. III. Further developments of the boson polynomials and their implications, J. Math. Phys. 14 (1973), 1336-1357.
24. T.H. Seligman, "Double Coset Decompositions of Finite Groups and the Many-Body Problem", Burg Verlag, A.G. Basel (1975).
25. C.W. Patterson and W.G. Harter, "Canonical symmetrization for the unitary bases. I. Canonical Weyl bases, J. Math. Phys. 17 (1976), 1125-1136; II. Boson and fermion bases, ibid, 17, 1137-1142.
26. J.S. Frame, G. de B. Robinson and R.M. Thrall, "The Hook Graphs of the Symmetric Group", Can. J. Math. 6, 316-324 (1954).
27. G. de B. Robinson, "Representation Theory of the Symmetric Group," University of Toronto Press, 1961.